

Ab initio calculations of erbium crystal field splittings in oxide hosts

Yogendra Limbu,¹ Yueguang Shi,¹ Joseph Sink,¹ Tharnier O. Puel,¹ Durga Paudyal,^{1,2,3} and Michael E. Flatté^{1,4}

¹*Department of Physics and Astronomy, University of Iowa, Iowa City, Iowa 52242, USA*

²*Ames National Laboratory of the US DOE, Iowa State University, Ames, IA 50011, USA*

³*Department of Electrical and Computer Engineering, Iowa State University, Ames, IA 50011, USA*

⁴*Department of Applied Physics, Eindhoven University of Technology, Eindhoven, The Netherlands*

We present an effective *ab initio* method to calculate the crystal field coefficients of an erbium (Er^{3+}) ion experiencing different local site symmetries in several wide-band-gap oxides, and then evaluate crystal field splittings of these Er^{3+} ions for their ground and excited states. The optical transitions between the ground state (Z) and excited state (Y) manifolds of the environmentally shielded $4f$ states of these Er^{3+} ions have wavelengths $\sim 1.5 \mu\text{m}$ and thus have potential applications to quantum communications and quantum memories. These results are in excellent agreement with recent low-temperature measurements, provided the inadequate calculation of the $4f$ shell screening is adjusted by reducing the radial extent of the $4f$ wavefunctions by approximately a factor of 2.

Rare earth (RE) ions, substituted in wide band gap insulating materials [1–3], can enhance the efficiency and speed of quantum information transmission over long distances and thus enable advances in quantum information science (QIS) [4–8]. The crystal field splitting of localized $4f$ electrons causes sharp optical, electric, and magnetic dipole transitions [9] favorable for QIS. The $4f$ transitions of Er^{3+} ions draw particular attention due to long optical and spin coherence times, controllable $4f$ linewidth broadening, and emission in the telecommunications band [1, 2, 4]. The Er^{3+} ion, which emits a light of $\sim 1.5 \mu\text{m}$ from the $4f - 4f$ transition [10], has diverse applications when hosted in wide band gap oxides, e.g., Y_2SiO_5 for quantum memory [11–13] and Y_2O_3 for spin-photon interfaces [14, 15]. When rare earth atoms are embedded into a host material, the lowered symmetry splits the high angular-momentum energy levels of the isolated atom into sets of multiplets [16]. For example, the ubiquitous Er^{3+} ion, which has a vacuum ground state with $^4\text{I}_{15/2}$ character (Z manifold) and excited state with $^4\text{I}_{13/2}$ character (Y manifold), often splits into eight ground-state ($Z_1 - Z_8$) and seven excited-state doublets ($Y_1 - Y_7$). As quantum-coherent phenomena often require controlled optical coupling between individual states, *i.e.* a $Y_1 \rightarrow Z_1$ transition, knowledge of the crystal field splittings (CFS) informs decisions about bandwidth, cooling requirements, and performance for quantum operations. Current experimental literature relies on solving an effective total Hamiltonian iteratively to fit crystal field coefficients (CFCs) [17, 18]. There is a critical need to accurately predict CFCs and CFSs of RE ions hosted in wide-band-gap materials, preferably from *ab initio* calculations with a minimal number of adjustable parameters. Development of a universal method is especially desirable so that inverse design techniques can identify potential QIS materials from predicted CFCs and crystal field splittings.

Here we report the development of an effective method of calculating CFCs of Er doped into wide band gap oxides from *ab initio* (density functional theory, DFT) cal-

culations. Comparison with recent low-temperature measurements [4] of CFSs of Er in MgO , TiO_2 , ZnO , CaWO_4 , and PbWO_4 show excellent agreement if the radial extent of the $4f$ wavefunction is modified by a single factor ~ 2 , which is nearly identical across these materials, and represents the limitation of DFT in calculating the radius of the strongly-correlated, partially-filled $4f$ shell of Er.

Calculations of CFCs from DFT [19–22] have been attempted before, however complexities arise from $4f-4f$ self interaction and hybridization of $4f$ states with other states. This problem can partially be resolved by placing the $4f$ electrons in the core, forcing their electron density to have spherical symmetry [19–21]. Some [19–21] have introduced an empirical parameter to remove the hybridization between $4f$ states and other states using a Wannier function analysis. The empirical parameter is very different for different RE ions and its determination requires delicate analysis of the hybridization emerging from the calculation. An alternative method relies on an effective core potential using Gaussian basis sets [22], however the $4f$ tail may still hybridize unphysically with other valence states, requiring an additional density-dependent pseudopotential term. Here we calculate the CFCs within the $4f$ core approximation using a single physically-justifiable adjustable parameter, $\epsilon_{\omega,q}$, the dielectric constant.

Once these CFCs are obtained the lanthanide ion energy spectrum was calculated using the *qlanth* code [23], which includes terms representing the following interactions and relativistic corrections: spin-orbit, electrostatic repulsion, spin-spin, crystal field and spin-other-orbit as described in [17]. *qlanth* now has major improvements over previous versions (*i.e.* Ref. [24]); it has fixed errors found in the term that includes configuration interaction via the Casimir operator of $\text{SO}(3)$, has implemented the non-orthogonal terms for the three-body effective operators as discussed in [25], has corrected some typos as well as improved accuracy in the Marvin integral terms, and implemented significant optimizations in the code itself. With these changes *qlanth* reproduces the CFSs of

Ref. [17] with an agreement ($\lesssim 30 \text{ cm}^{-1}$ throughout all lanthanides).

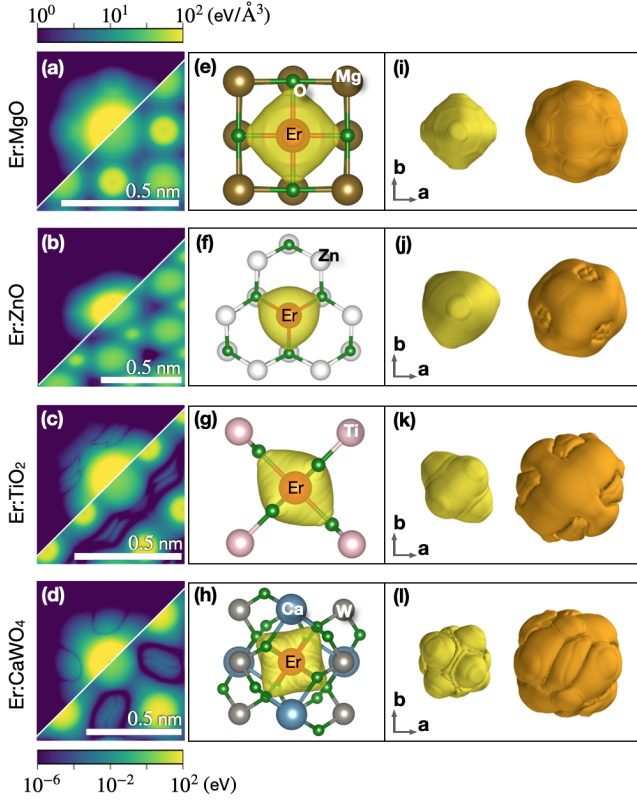


FIG. 1. (a)-(d) Two-dimensional views of the crystal field potential $V_{CF}(\mathbf{r})$ and the same potential multiplied by the $4f$ -electrons probability density of Er (upper diagonal, in $\text{eV}/\text{\AA}^3$). (e)-(h) show the crystal structure surrounding the doped Er ion and the probability density of the $4f$ -electrons at $1.58 \text{ eV}/\text{\AA}^3$ (yellow isocontour); (i)-(l) illustrate the probability density by plotting it at $10^{-2} \text{ eV}/\text{\AA}^3$ (left) and $10^{-6} \text{ eV}/\text{\AA}^3$ (right) isocontours, omitting the depiction of the crystal.

The effective Hamiltonian of a single RE atom in the crystal environment is [19, 20]: $H_{\text{eff}} = H_{FI} + H_{CF}$, where H_{FI} and H_{CF} are free ion and one-particle crystal field Hamiltonians. The free ion Hamiltonian of $4f^N$ configuration, including two and three body operators in the configuration interactions is [17]: $H_{FI} = H_0 + \sum_k F^k f_k + \zeta_{4f} A_{SO} + \alpha L(L+1) + \beta G(G_2) + \gamma G(G_7) + \sum_i t_i T^i + \sum_h m_h M^h + \sum_f p_f P^f$, where H_0 is spherically symmetric one-electron Hamiltonian, F^k and f_k ($k = 0, 2, 4, 6$) are electrostatic integral and angular part of the electrostatic interaction in two-body configuration, ζ_{4f} and A_{SO} are spin-orbit integral and angular part of spin-orbit interaction, α , β , and γ are the Trees parameters (correction terms, which are obtained from *ab initio* method or fitting experimental data [17]) associated with the two-body interaction operators [26, 27], and $G(G_2)$ and $G(G_7)$ are the eigenvalues of Casimir's operators for the groups G_2 and G_7 , whereas L is total orbital angular momentum [26, 28]. For the three

or more $4f$ electrons, the three-particle configuration interaction is included by adding $t_i T^i$ ($i = 2, 3, 4, 6, 7, 8$) in two particles Hamiltonian [26, 29], where T^i are the adjustable parameters, which are obtained from *ab initio* method or fitting experimental data [17, 30], and t_i are three-particle operators. These atomic parameters are extracted from Ref. [17]. Further, M_h ($h = 0, 2, 4$) contains spin-spin and spin-other-orbit relativistic corrections, known as Marvin integrals [31], while P^f ($f = 2, 4, 6$) represents the electrostatically correlated spin-orbit perturbation of two-body magnetic corrections. m_h and p^f are operators associated with these magnetically correlated corrections.

The crystal field potential [28] is: $V_{CF} = \sum_{k,q} B_q^k(r) C_q^k(\theta, \phi)$, where $B_q^k(r)$ and $C_q^k(\theta, \phi)$ are the radial and spherical components of V_{CF} . The position independent B_q^k coefficients, which depend on the local site symmetry of RE ion in the crystal [17, 22] are:

$$B_q^k = \frac{2k+1}{4\pi} \int V_{CF}(r, \theta, \phi) R_{4f}^2(r) C_q^{k*}(\theta, \phi) r^2 dr \sin \theta d\theta d\phi,$$

where $R_{4f}^2(r)$ and $C_q^{k*}(\theta, \phi)$ indicate the square of the $4f$ radial wave function and the complex conjugate of the spherical tensor. The $4f$ radial wave function of the RE ion, which depends on the dielectric constant of the material and position of $4f$ electrons is: $R_{4f}(r, \epsilon_{\omega, \mathbf{q} \sim a_0}) = A r^3 e^{-r Z_{\text{eff}}/n a_0 \epsilon_{\omega, \mathbf{q}}}$, where A , n , a_0 , and Z_{eff} are the amplitude of $4f$ wave function, principal quantum number, the Bohr radius, and effective nuclear charge of $4f$ orbital, respectively, in the RE ion. The orbital exponent of $4f$ electron ($\zeta_{n,l,m}$) of Er, which is related to the screening constant, is taken from Ref. [32] for calculating the effective nuclear charge of $4f$ orbital using relation $Z_{\text{eff}} = n \zeta_{n,l,m}$, yielding a value of 27.9784. Here the dielectric constant, $\epsilon_{\omega, \mathbf{q}}$, which depends upon the frequency and crystal structure, and controls the spreading of the $4f$ radial wave function, is carefully optimized by fitting the calculated and the experimental energy levels. The optimized $\epsilon_{\omega, \mathbf{q}}$ for MgO, ZnO, TiO₂, PbWO₄, and CaWO₄ are 1.96, 1.90, 2.00, 2.24, and 2.24, respectively. The corresponding $\epsilon_{\omega, \mathbf{q}}$ are then used to extract CFCs from the self-consistent DFT charge densities and local potentials.

In addition, we performed maximally localized Wannier functions (Wannier90 [33]) calculations and extracted maximally-localised Wannier $4f$ functions with $4f$ electrons as valence electrons. These extracted $4f$ Wannier functions are then compared with hydrogenic $4f$ radial wave functions for different values of $\epsilon_{\omega, \mathbf{q}}$. The extracted Wannier function is in good agreement with the hydrogenic wave function when epsilon is in between 3 and 4. This is also confirmed by the ionization energy of Er^{3+} ($\sim 42.42 \text{ eV}$ [34, 35]), which is expressed as, $E_i = m_e e^4 Z_{\text{eff}}^2 / (4\pi \epsilon_{\text{eff}})^2 \hbar^2 n^2$, where m_e and $\epsilon_{\text{eff}} (= \epsilon_{\omega, \mathbf{q}} \epsilon_0)$ are the electron mass and permittivity. The resulting dielectric constant, $\epsilon_{\omega, \mathbf{q}}$, is 3.96 in agreement with the Wannier90 value (Fig. 3 [36]).

B_q^k	MgO	ZnO	TiO ₂	CaWO ₄	PbWO ₄
B_0^2		-260.96	74.19	846.34	872.91
$B_{\pm 2}^2$			$\pm i474.97$		
B_0^4	660.96	199.04	-493.49	187.43	90.08
$B_{\pm 2}^4$			$\pm i146.80$		
$B_{\pm 3}^4$		-i92.07			
$B_{\pm 4}^4$	395.00		310.25	$\begin{pmatrix} 192.40 \\ \mp i56.58 \end{pmatrix}$	$\begin{pmatrix} 114.55 \\ \pm i2.79 \end{pmatrix}$
B_0^6	-78.57	-240.17	466.69	87.40	138.50
$B_{\pm 2}^6$			$\pm i85.65$		
$B_{\pm 3}^6$		-i228.92			
$B_{\pm 4}^6$	146.98		106.82	$\begin{pmatrix} 311.06 \\ \mp i424.36 \end{pmatrix}$	$\begin{pmatrix} 182.07 \\ \mp i352.72 \end{pmatrix}$
$B_{\pm 6}^6$		233.60	$\pm i254.93$		

TABLE I. extracted CFCs (units of cm^{-1}) of Er doped in wide band gap oxides with variable local site symmetry, e.g., MgO with O_h , ZnO with C_{3v} , TiO₂ with D_{2h} , and CaWO₄ and PbWO₄ with S_4 , from DFT calculations.

The DFT calculations are performed using the Vienna *Ab-initio* Simulation Package [37, 38]. Augmented plane wave pseudopotentials [39] and Perdew-Burke-Ernzerhof functionals [40] are used. A sufficient plane wave cut off energy (500 eV) and Γ centered k -mesh (maximum of $10 \times 10 \times 10$) are used for the Brillouin zone sampling. The $4f$ electrons are frozen in the core and the $6s^2$, $5p^6$, and $5d^1$ electrons are considered in the valance shell. From non-spin polarized calculations the self-consistent charge densities and local potentials were generated to produce the B_q^k considering the local potentials as crystal fields.

In order to study the crystal field splitting of $4f$ states of Er^{3+} ions, we focused on the oxides MgO, ZnO, TiO₂, CaWO₄ and PbWO₄, with variable point group symmetry. MgO, ZnO, and TiO₂ have cubic, hexagonal, and rutile (tetragonal) crystal structures with O_h , C_{6v} , and D_{4h} point groups and $Fm\bar{3}m$, $P6_3mc$, and $P4_2/mnm$ space groups, respectively, whereas both CaWO₄ and PbWO₄ have tetragonal crystal structure with C_{4h} point and $I4_1/a$ space groups. The optimized lattice parameters for MgO ($a = 4.24$ Å), ZnO ($a = 3.28$ Å and $c = 5.30$ Å), TiO₂ ($a = 4.66$ Å and $c = 2.96$ Å), CaWO₄ ($a = 5.29$ Å and $c = 11.43$ Å), and PbWO₄ ($a = 5.51$ Å and $c = 12.13$ Å) are in good agreement with the available literature [41–45].

Calculated band gaps for TiO₂, CaWO₄, and PbWO₄ from a standard hybrid functional (HSE06) are 3.04, 5.39, and 4.30 eV (Fig. 4 [36]), which are in good agreement with the corresponding experiments [46–48]. However, the standard hybrid functional was unable to reproduce the experimental band gaps of MgO and ZnO. In these cases, the hybrid functional calculations with Hartree Fock mixing parameters of 0.45 for MgO and 0.38 for ZnO show band gaps of 7.65 eV and 3.31 eV (Fig. 4 [36]),

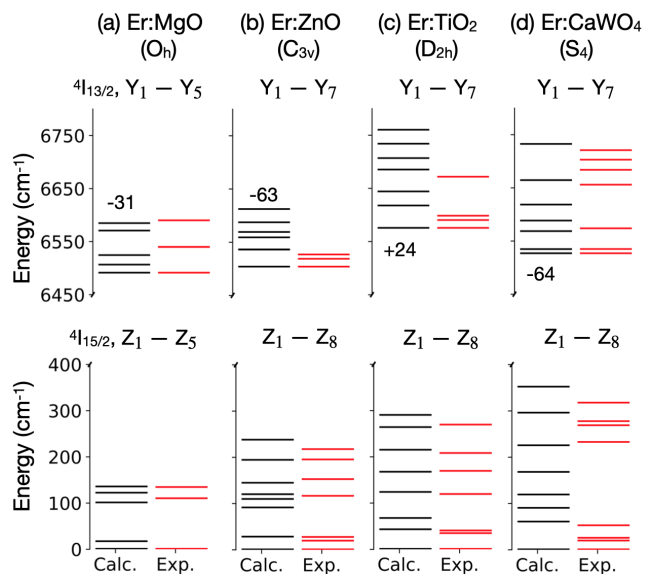


FIG. 2. The ground ($^4I_{15/2}$) and first excited ($^4I_{13/2}$) multiplets splittings of the $4f$ states of Er^{3+} ion in (a) MgO, (b) ZnO, (c) TiO₂, and (d) CaWO₄. The eight Kramers-pairs levels from the ground state, $Z_1 - Z_8$, and seven levels from the first excited state of Er^{3+} , $Y_1 - Y_7$, are identified in all cases, except for MgO, in which the multiplet is split into five energy levels. In the $^4I_{13/2}$ splittings, we have adjusted the calculated values to aligned with the Y_1 experimental values (e.g., -31 cm^{-1} for Er:MgO), as the gap between the multiplets is not a property from the crystal field and can be adjusted with the Er ion parameters.

which are indeed in good agreement with corresponding experiment [49, 50]. These wide band gap non magnetic host oxides with nuclear spin-free isotopes [4] become excellent hosts for Er^{3+} ions to provide sharp $4f - 4f$ transitions, exhibiting long spin and optical coherence times needed for quantum storage and spin-photon interface.

Now we describe CFCs calculations and results using Wybourne notation and cm^{-1} units [28]. In MgO, the Er site has O_h local site symmetry [51, 52]. From group theory, only the B_q^k for $k = 4$ and 6 , and $q = 0$ and ± 4 are non-zero, satisfying the relations $B_{\pm 4}^4 = \sqrt{\frac{5}{14}}B_0^4$ and $B_{\pm 4}^6 = -\sqrt{\frac{7}{2}}B_0^6$ [22]. All CFCs are positive, except for B_0^6 . In CaWO₄ and PbWO₄, the Er doped site favors S_4 local site symmetry [53]. Five non-zero CFCs: B_0^2 , B_0^4 , $B_{\pm 4}^4$, B_0^6 , and $B_{\pm 4}^6$ are identified in both materials as also suggested in Refs. [21, 54]. The $B_{\pm 4}^4$ and $B_{\pm 4}^6$ have real and imaginary components, while B_0^2 , B_0^4 , and B_0^6 have only the real components. The real components of CFCs follow the relation $\text{Re}[B_q^k] = \text{Re}[B_{-q}^k]$, whereas the imaginary components follow the relation, $\text{Im}[B_{-q}^k] = -\text{Im}[B_q^k]$, except for $B_{\pm 4}^4$ in PbWO₄ with $\text{Im}[B_{-q}^k] = \text{Im}[B_q^k]$. In ZnO, Er doped site favors C_{3v} local site symmetry [4]. Six non-zero CFCs: B_0^2 , B_0^4 , $B_{\pm 3}^4$, B_0^6 , $B_{\pm 3}^6$, and $B_{\pm 6}^6$ are deduced as described in Refs. [28, 55]. The coefficients:

$B_{\pm 3}^4$ and $B_{\pm 3}^6$ have only the imaginary components with the relation $\text{Im}[B_q^k] = \text{Im}[B_{-q}^k]$. In TiO_2 , Er doped site has D_{2h} local site symmetry [56]. In this case, there are five real and four imaginary CFCs as also mentioned in Ref. [57]. The real CFCs are B_0^2 , B_0^4 , $B_{\pm 4}^4$, B_0^6 , and $B_{\pm 4}^6$ and the imaginary CFCs are $B_{\pm 2}^2$, $B_{\pm 2}^4$, $B_{\pm 2}^6$, and $B_{\pm 6}^6$. The real and imaginary components follow the relation $\text{Re}[B_q^k] = \text{Re}[B_{-q}^k]$ and $\text{Im}[B_q^k] = -\text{Im}[B_{-q}^k]$. Thus, in S_4 , D_{2h} , and C_{3v} local site symmetries, the $4f$ splitting of Er^{3+} ions are due to the second, fourth, and sixth order CFCs, whereas in O_h local site symmetry, the $4f$ splitting of Er^{3+} ion is due to the fourth and sixth order CFCs.

The $4f$ states of Er^{3+} with O_h local site symmetry splits the ground state into three quartets Γ_8 (0.00, 17.37, and 122.52 cm^{-1}) and two doublets Γ_7 (101.32 cm^{-1}) and Γ_6 (135.95 cm^{-1}) (Fig. 6 [36]) as also suggested in Refs. [51, 58] and observed experimentally [4] (Fig. 2(a)). We note that the order and position of doublets and quartets are sensitive to the ratio of fourth and sixth order CFCs [59, 60]. We followed the irreducible representation mentioned in Ref. [61]. Similarly, two quartets (6537.66 and 6615.81 cm^{-1}) and three doublets (6522.43 cm^{-1} (Γ_6), and 6555.57 and 6601.82 cm^{-1} (Γ_7)) are identified in the first excited state. The $4f - 4f$ transition from Y_1 to Z_1 is 6522.43 cm^{-1} . Without crystal field environment, the calculated $4f - 4f$ transition from the first excited state to the ground state is 6488.00 cm^{-1} (6478.00 cm^{-1} in the experiment [53]), which is 34.43 cm^{-1} shorter than that of with the crystal field environment. This indeed shows the increase of wave length when the crystal environment is neglected.

In Er doped ZnO with C_{3v} symmetry, the $4f$ states of Er^{3+} ion splits into three $\Gamma_{5,6}$ and five Γ_4 Kramers doublets in the ground state (Fig. 6 [36]), which are in good agreement with the experiment (Fig. 2(b)). Here, Γ_5 and Γ_6 form a doublet, while Γ_4 forms a separate doublet. In the ground state, the energy levels Z_1 , Z_4 , and Z_7 correspond to $\Gamma_{4,5}$, and the remaining energy levels Z_2 , Z_3 , Z_5 , Z_6 , and Z_8 correspond to Γ_4 . Similarly, seven energy levels, $2\Gamma_{4,5} + 5\Gamma_4$, are found in the first excited state (Fig. 2(b)), where Y_2 and Y_6 are $\Gamma_{5,6}$, and the remaining Y_1 , Y_3 , Y_5 , and Y_7 are Γ_4 . In the experiment, only seven and three multiplets are visualized in the ground and first excited states [4]. The calculated $4f - 4f$ transition from Y_1 to Z_1 is 6567.52 cm^{-1} , which is 63.32 cm^{-1} larger than the experiment [4].

Er doping in TiO_2 has D_{2h} local site symmetry. The $4f$ states form eight and seven Kramers doublets as represented by Γ_5 (Fig. 6 [36]) as mentioned in Ref. [62] in the ground and first excited states, which are in fair agreement with the experiment [4, 63] (Fig. 2(c)). In the experiment, only seven and four multiplets are observed in the ground and first excited states [4, 63]. The $4f - 4f$ transition from Y_1 to Z_1 is 6552.43 cm^{-1} , which is (23.27 cm^{-1}) smaller than the experiment [4]. The D_{2h} local site symmetry does not allow a permanent electric

dipole moment [4, 63], revealing the $4f - 4f$ transition is mainly due to magnetic dipole transition.

In the case of Er doped CaWO_4 with S_4 local site symmetry, the $4f$ states also form eight ($4\Gamma_{5,6} + 4\Gamma_{7,8}$) and seven ($4\Gamma_{5,6} + 3\Gamma_{7,8}$) Kramers doublets in the ground and first excited states (Fig. 6 [36]), which are also in fair agreement with the experiment [54] (Fig. 2(d)). In the ground state, the energy levels Z_1 , Z_3 , Z_6 , and Z_7 are $\Gamma_{5,6}$, while the other four states Z_2 , Z_4 , Z_5 , and Z_8 are $\Gamma_{7,8}$. The energy levels Y_1 , Y_3 , Y_6 , and Y_7 correspond to $\Gamma_{5,6}$, while the other three states Y_2 , Y_4 , and Y_5 are $\Gamma_{7,8}$ in the first excited state. The $4f - 4f$ transition from Y_1 to Z_1 is 6591.30 cm^{-1} , which is 64.30 cm^{-1} larger than the experiment [54] (Fig. 2(d)). PbWO_4 has the same crystal structure as CaWO_4 . Thus, eight and seven Kramers doublets are identified in the ground and first excited states. The $4f - 4f$ transition from Y_1 to Z_1 is 6570.05 cm^{-1} , which shows a good agreement with experiment [4].

In conclusion, we have developed an effective *ab initio* method of calculating crystal field coefficients and energy splitting of $4f$ states of Er^{3+} ions in wide band gap oxides with different local site symmetries, e.g., O_h , C_{3v} , D_{2h} , and S_4 . The calculated band gaps of representative oxides with different point group symmetry, such as MgO with O_h , ZnO with C_{6v} , CaWO_4 and PbWO_4 with C_{4h} , and TiO_2 with D_{4h} , using density functional theory (DFT) incorporating a fraction of exact exchange, are in good agreement with available experimental values. The crystal field coefficients of Er^{3+} ions in these oxides are extracted from self-consistent charge densities of non spin polarized DFT calculations within the core approximation. These coefficients are then fed into an effective Hamiltonian to generate the crystal field splitting of Er^{3+} . The resulting crystal field multiplets are in good agreement with available experimental values. Further details of the calculations presented here are available in a simultaneously submitted publication[64].

This work is supported by the U.S. Department of Energy, Office of Science, Office of Basic Energy Sciences under Award Number DE-SC0023393.

-
- [1] Gregory D. Grant, Jiefei Zhang, Ignas Masiulionis, Swarnabha Chattaraj, Kathryn E. Sautter, Sean E. Sullivan, Rishi Chebrolu, Yuzi Liu, Jessica B. Martins, Jens Niklas, Alan M. Dibos, Sumit Kewalramani, John W. Freeland, Jianguo Wen, Oleg G. Poluektov, F. Joseph Heremans, David D. Awschalom, and Supratik Guha, "Optical and microstructural characterization of Er^{3+} doped epitaxial cerium oxide on silicon," *APL Mater.* **12**, 021121 (2024).
 - [2] Charles W. Thiel, Thomas Böttger, and R. L. Cone, "Rare-earth-doped materials for applications in quantum information storage and signal processing," *J. Lumin.* **131**, 353–361 (2011).

- [3] R. Kolesov, K. Xia, R. Reuter, R. Stöhr, A. Zappe, J. Meijer, P. R. Hemmer, and J. Wrachtrup, “Optical detection of a single rare-earth ion in a crystal,” *Nat. Commun.* **3**, 1029 (2012).
- [4] Paul Stevenson, Christopher M. Phenicie, Isaiah Gray, Sebastian P. Horvath, Sacha Welinski, Austin M. Ferrenti, Alban Ferrier, Philippe Goldner, Sujit Das, Ramamoorthy Ramesh, Robert J. Cava, Nathalie P. de Leon, and Jeff D. Thompson, “Erbium-implanted materials for quantum communication applications,” *Phys. Rev. B* **105**, 224106 (2022).
- [5] Tian Zhong and Philippe Goldner, “Emerging rare-earth doped material platforms for quantum nanophotonics,” *Nanophotonics* **8**, 2003–2015 (2019).
- [6] Nathalie Kunkel, Alban Ferrier, Charles W. Thiel, Mariola O. Ramírez, Luisa E. Bausá, Rufus L. Cone, Akio Ikesue, and Philippe Goldner, “Rare-earth doped transparent ceramics for spectral filtering and quantum information processing,” *APL Mater.* **3**, 096103 (2015).
- [7] Cheng Ji, Michael T. Solomon, Gregory D. Grant, Koichi Tanaka, Muchuan Hua, Jianguo Wen, Sagar Kumar Seth, Connor P. Horn, Ignas Masiulionis, Manish Kumar Singh, Sean E. Sullivan, F. Joseph Heremans, David D. Awschalom, Supratik Guha, and Alan M. Dibos, “Nanocavity-mediated Purcell enhancement of Er in TiO₂ thin films grown via atomic layer deposition,” *ACS Nano* **18**, 9929 (2024).
- [8] A. J. Kenyon, “Recent developments in rare-earth doped materials for optoelectronics,” *Prog. Quantum Electron.* **26**, 225–284 (2002).
- [9] Guokui Liu and Bernard Jacquier, *Spectroscopic Properties of Rare Earths in Optical Materials* (Springer, 2005).
- [10] Boris Ivanovich Galagan, Boris I. Denker, Vyacheslav V. Osiko, and Sergei E. Sverchkov, “Spectral and kinetic properties of Er³⁺, Yb³⁺:Yb₃Al₅O₁₂ crystals at high temperatures,” *Quantum Electron.* **36**, 595 (2006).
- [11] C. W. Thiel, W. R. Babbitt, and R. L. Cone, “Optical decoherence studies of yttrium oxyorthosilicate Y₂SiO₅ codoped with Er³⁺ and Eu³⁺ for optical signal processing and quantum information applications at 1.5 microns,” *Phys. Rev. B* **85**, 174302 (2012).
- [12] Hee-Jin Lim, Sacha Welinski, Alban Ferrier, Philippe Goldner, and J. J. L. Morton, “Coherent spin dynamics of ytterbium ions in yttrium orthosilicate,” *Phys. Rev. B* **97**, 064409 (2018).
- [13] Pierre Jobez, Cyril Laplane, Nuala Timoney, Nicolas Gisin, Alban Ferrier, Philippe Goldner, and Mikael Afzelius, “Coherent spin control at the quantum level in an ensemble-based optical memory,” *Phys. Rev. Lett.* **114**, 230502 (2015).
- [14] Churna Bhandari, Cüneyt Şahin, Durga Paudyal, and Michael E. Flatté, “Distinguishing erbium dopants in Y₂O₃ by site symmetry: *Ab initio* theory of two spin-photon interfaces,” *Phys. Rev. Mater.* **7**, 126201 (2023).
- [15] Yuanbing Mao, Jian Y. Huang, Roman Ostroumov, Kang L. Wang, and Jane P. Chang, “Synthesis and luminescence properties of erbium-doped Y₂O₃ nanotubes,” *J. Phys. Chem. C* **112**, 2278–2285 (2008).
- [16] Mildred S. Dresselhaus, Gene Dresselhaus, and Ado Jorio, “Group theory: Application to the physics of condensed matter,” (2007).
- [17] W. T. Carnall, G. L. Goodman, K. Rajnak, and R. S. Rana, “A systematic analysis of the spectra of the lanthanides doped into single crystal LaF₃,” *J. Chem. Phys.* **90**, 3443–3457 (1989).
- [18] Chang-kui Duan, Peter A. Tanner, Vladimir N. Makhov, and Marco Kirm, “Vacuum ultraviolet spectra and crystal field analysis of YAlO₃ doped with Nd³⁺ and Er³⁺,” *Phys. Rev. B* **75**, 195130 (2007).
- [19] P. Novák, K. Knížek, M. Maryško, Z. Jiráček, and J. Kuneš, “Crystal field and magnetism of Pr³⁺ and Nd³⁺ ions in orthorhombic perovskites,” *J. Phys. Condens. Matter* **25**, 446001 (2013).
- [20] P. Novák, K. Knížek, and J. Kuneš, “Crystal field parameters with Wannier functions: Application to rare-earth aluminates,” *Phys. Rev. B* **87**, 205139 (2013).
- [21] Leila Mollabashi and S. Jalali-Asadabadi, “Crystal fields of lithium rare-earth tetrafluorides and multiplet splitting of the +3 rare-earth ions,” *Phys. Rev. B* **102**, 045120 (2020).
- [22] Lixin Ning and Gian Paolo Brivio, “Density functional theory calculation of crystal-field energy levels for Yb³⁺ in the Cs₂NaYbF₆ crystal,” *Phys. Rev. B* **75**, 235126 (2007).
- [23] Juan David Lizarazo Ferro, “qlanth: A hamiltonian for the lanthanides.” San Francisco (CA): GitHub (2024).
- [24] Christopher M. Dodson and Rashid Zia, “Magnetic dipole and electric quadrupole transitions in the trivalent lanthanide series: Calculated emission rates and oscillator strengths,” *Phys. Rev. B* **86**, 125102 (2012).
- [25] B. R. Judd and H. Crosswhite, “Orthogonalized operators for the *f* shell,” *J. Opt. Soc. Am. B* **1**, 255–260 (1984).
- [26] K. Rajnak and B. G. Wybourne, “Configuration interaction effects in *l^N* configurations,” *Phys. Rev.* **132**, 280 (1963).
- [27] R. E. Trees, “Configuration interaction in Mn II,” *Phys. Rev.* **83**, 756 (1951).
- [28] Brian G. Wybourne, *Spectroscopic properties of rare earths* (Interscience, 1965).
- [29] B. R. Judd, “Three-particle operators for equivalent electrons,” *Phys. Rev.* **141**, 4 (1966).
- [30] W. T. Carnall, Hannah Crosswhite, and Henry Milton Crosswhite, *Energy level structure and transition probabilities in the spectra of the trivalent lanthanides in LaF₃*, Tech. Rep. ANL-78-XX-95 (Chemistry Division, Argonne National Laboratory, and Department of Physics, The Johns Hopkins University, 1978).
- [31] H. H. Marvin, “Mutual magnetic interactions of electrons,” *Phys. Rev.* **71**, 102 (1947).
- [32] Enrico Clementi, D. L. Raimondi, and William P. Reinhardt, “Atomic screening constants from SCF functions. II. atoms with 37 to 86 electrons,” *J. Chem. Phys.* **47**, 1300–1307 (1967).
- [33] Arash A. Mostofi, Jonathan R. Yates, Young-Su Lee, Ivo Souza, David Vanderbilt, and Nicola Marzari, “wannier90: A tool for obtaining maximally-localised Wannier functions,” *Comput. Phys. Commun.* **178**, 685–699 (2008).
- [34] David A. Johnson and Peter G. Nelson, “Lanthanide ionization energies and the sub-shell break. Part 2. The third and fourth ionization energies,” *J. Phys. Chem. Ref. Data* **46**, 013109 (2017).
- [35] Peter F. Lang and Barry C. Smith, “Ionization energies of lanthanides,” *J. Chem. Educ.* **87**, 875–881 (2010).
- [36] Yogendra Limbu, Yueguang Shi, Joseph Sink, Tharnier O. Puel, Durga Paudyal, and Michael E. Flatté, “*Ab Initio* crystal field theory: Erbium in oxide

- hosts for quantum applications,” Submitted to Phys. Rev. B (2024).
- [37] Jürgen Hafner, “*Ab-initio* simulations of materials using VASP: Density-functional theory and beyond,” *J. Comput. Chem.* **29**, 2044–2078 (2008).
- [38] Georg Kresse and Jürgen Furthmüller, “Efficiency of *ab-initio* total energy calculations for metals and semiconductors using a plane-wave basis set,” *Comput. Mater. Sci.* **6**, 15–50 (1996).
- [39] Peter E. Blöchl, “Projector augmented-wave method,” *Phys. Rev. B* **50**, 17953 (1994).
- [40] Matthias Ernzerhof and Gustavo E. Scuseria, “Assessment of the Perdew–Burke–Ernzerhof exchange-correlation functional,” *J. Chem. Phys.* **110**, 5029–5036 (1999).
- [41] Norina A. Richter, Sabrina Siculo, Sergey V. Levchenko, Joachim Sauer, and Matthias Scheffler, “Concentration of vacancies at metal-oxide surfaces: Case study of MgO (100),” *Phys. Rev. Lett.* **111**, 045502 (2013).
- [42] B. Meyer and Dominik Marx, “Density-functional study of the structure and stability of ZnO surfaces,” *Phys. Rev. B* **67**, 035403 (2003).
- [43] L. S. Cavalcante, V. M. Longo, J. C. Sczancoski, M. A. P. Almeida, A. A. Batista, José Arana Varela, Marcelo Ornanghi Orlandi, Elson Longo, and M. Siu Li, “Electronic structure, growth mechanism and photoluminescence of CaWO₄ crystals,” *CrystEngComm* **14**, 853–868 (2012).
- [44] Yaoju Zhang, N. A. W. Holzwarth, and R. T. Williams, “Electronic band structures of the scheelite materials CaMoO₄, CaWO₄, PbMoO₄, and PbWO₄,” *Phys. Rev. B* **57**, 12738 (1998).
- [45] Wolfgang Körner and Christian Elsässer, “Density functional theory study of dopants in polycrystalline TiO₂,” *Phys. Rev. B* **83**, 205315 (2011).
- [46] V. B. Mikhailik, H. Kraus, D. Wahl, M. Itoh, M. Koike, and I. K. Bailiff, “One- and two-photon excited luminescence and band-gap assignment in CaWO₄,” *Phys. Rev. B* **69**, 205110 (2004).
- [47] R. Lacomba-Perales, J. Ruiz-Fuertes, D. Errandonea, D. Martínez-García, and A. Segura, “Optical absorption of divalent metal tungstates: correlation between the band-gap energy and the cation ionic radius,” *EPL* **83**, 37002 (2008).
- [48] Nick Serpone, “Is the band gap of pristine TiO₂ narrowed by anion- and cation-doping of titanium dioxide in second-generation photocatalysts?” *J. Phys. Chem. B* **110**, 24287–24293 (2006).
- [49] R. C. Whited, Christopher J. Flaten, and W. C. Walker, “Exciton thermorefectance of MgO and CaO,” *Solid State Commun.* **13**, 1903–1905 (1973).
- [50] Vedentam Srikant and David R. Clarke, “On the optical band gap of zinc oxide,” *J. Appl. Phys.* **83**, 5447–5451 (1998).
- [51] M. Borg, R. Buisson, and C. Jacolin, “Spin-lattice relaxation in a Γ_8 quartet: Er³⁺ in MgO,” *Phys. Rev. B* **1**, 1917 (1970).
- [52] J. M. Baker and G. Currell, “Orbit-lattice interaction in Γ_8 quartets. I. determination of the coupling parameters for Er³⁺:MgO and Dy³⁺:CaF₂ from EPR under uniaxial stress,” *J. Phys. C: Solid State Phys.* **9**, 3819 (1976).
- [53] Bernal G. Enrique, “Optical spectrum and magnetic properties of Er³⁺ in CaWO₄,” *J. Chem. Phys.* **55**, 2538–2549 (1971).
- [54] Donald E. Wortman, “Optical spectrum of triply ionized erbium in calcium tungstate,” *J. Chem. Phys.* **54**, 314–321 (1971).
- [55] M. Diviš, J. Hölsä, M. Lastusaari, A. P. Litvinchuk, and V. Nekvasil, “Crystal field effect in YbMnO₃,” *J. Alloys Compd.* **451**, 662–665 (2008).
- [56] N. K. A. Hamed, N. Nafarizal, M. K. Ahmad, A. B. Faridah, and M. Shimomura, “Dominant co-exposed {101}/{111} facet of Er-doped rutile TiO₂ film via hydrothermal doping,” *Mater. Lett.* **336**, 133864 (2023).
- [57] A. Furrer, P. Brüesch, and P. Unternährer, “Neutron spectroscopic determination of the crystalline electric field in HoBa₂Cu₃O_{7- δ} ,” *Phys. Rev. B* **38**, 4616 (1988).
- [58] B. Bleaney, “A new class of materials for Bloembergen-type masers,” *Proc. Phys. Soc.* **73**, 937 (1959).
- [59] J. A. White, “Energy levels of rare earth ions in cubic crystal fields,” *J. Phys. Chem. Solids* **23**, 1787–1793 (1962).
- [60] S. C. Chen and D. J. Newman, “Superposition model of the orbit-lattice interaction. II. analysis of strain results for Er³⁺:MgO,” *J. Phys. C: Solid State Phys.* **17**, 3045 (1984).
- [61] C. J. Bradley and A. P. Cracknell, *The Mathematical Theory of Symmetry in Solids* (Oxford: Clarendon, 1972).
- [62] G. L. Goodman, C. K. Loong, and L. Soderholm, “Crystal field properties of f-electron states in RBa₂Cu₃O₇ for R = Ho, Nd and Pr,” *J. Phys.: Condens. Matter* **3**, 49 (1991).
- [63] Christopher M. Phenicie, Paul Stevenson, Sacha Welinski, Brendon C. Rose, Abraham T. Asfaw, Robert J. Cava, Stephen A. Lyon, Nathalie P. De Leon, and Jeff D. Thompson, “Narrow optical line widths in erbium implanted in TiO₂,” *Nano Lett.* **19**, 8928–8933 (2019).
- [64] Y. Limbu, Y. Shi, J. Sink, T. O. Puel, D. Paudyal, and M. E. Flatté, “*Ab initio* calculations of erbium crystal field splittings in oxide hosts: role of the 4f radial wave function,” (2025), unpublished.